

available at www.sciencedirect.comjournal homepage: www.elsevier.com/locate/chnjc**Article****Preparation of Bi-doped TiO₂ nanoparticles and their visible light photocatalytic performance**Haiyan Li ^{a,b}, Jinfeng Liu ^a, Junjie Qian ^a, Qiuye Li ^a, Jianjun Yang ^{a,*}^a Key Laboratory for Special Functional Materials, Henan University, Kaifeng 475004, Henan, China^b College of Chemistry and Chemical Engineering, Henan University, Kaifeng 475004, Henan, China**ARTICLE INFO****Article history:**

Received 24 February 2014

Accepted 21 April 2014

Published 20 September 2014

Keywords:

Hydrothermal method

Bismuth-doping

Titanium dioxide

Nanotube titanic acid

Oxygen vacancy

Visible light photocatalysis

ABSTRACT

Bi-doped TiO₂ photocatalysts were prepared by a hydrothermal method using nanotube titanic acid as the Ti precursor. The samples were characterized by X-ray diffraction, transmission electron microscopy, ultraviolet-visible diffuse reflectance spectroscopy, and X-ray photoelectron spectroscopy. Methyl orange (MO) was used as a model contaminant to evaluate the visible light photocatalytic activity of the Bi-doped TiO₂ samples. We found that the Bi ions did not incorporate into the TiO₂ lattice but instead existed in the form of BiOCl. The obtained BiOCl-composited TiO₂ samples exhibited remarkable photocatalytic activity under visible light irradiation for the photodegradation of MO. The sample obtained when the Bi/Ti molar ratio was 1% and the hydrothermal treatment temperature was 130 °C (BTO-130-1) showed the highest photocatalytic activity. Moreover, a possible mechanism was proposed and the enhanced photocatalytic activity was discussed. The as-prepared catalyst also showed high photocatalytic activity for the photodegradation of 4-chlorophenol.

© 2014, Dalian Institute of Chemical Physics, Chinese Academy of Sciences.

Published by Elsevier B.V. All rights reserved.

1. Introduction

Titanium dioxide (TiO₂), a promising semiconductor photocatalyst, has been intensely investigated for applications in air cleaning, water purification, and photocatalytic water splitting [1–3] because of its biological and chemical inertness, stability against photocorrosion and chemical corrosion, nontoxicity, and cost-effectiveness. Although TiO₂ generally shows high activity for the photocatalytic oxidation of organic pollutants [4], there are two drawbacks limiting its practical application: its low use of the solar spectrum (only active in the ultraviolet region) and its relatively high electron-hole recombination rate. To increase the photocatalytic efficiency of TiO₂, various methods have been used to enhance its absorption of the solar

spectrum and to inhibit the recombination of photogenerated electron-hole pairs. A prominent approach is to dope TiO₂ with transition metals (such as Fe, V and Cr) [5–7] or nonmetallic elements (such as N, C or B) [8–10]. Doping TiO₂ with metal ions has been investigated to expand the absorbance of TiO₂ into the visible region, and at suitable levels can inhibit electron-hole recombination [11]. Metal ion dopants may act as electron or hole traps and, consequently, alter the electron-hole recombination rate. Moreover, doping of TiO₂ with metal elements has been reported to be beneficial in narrowing its band gap. Indeed, doping TiO₂ with various metal ions has been found to improve its photocatalytic properties and enhance its response to visible light [12,13].

Recently, attention has been paid to TiO₂ nanopowders

* Corresponding author. Tel/Fax: +86-371-23881358; E-mail: yangjianjun@henu.edu.cn

This work was supported by the National Natural Science Foundation of China (20973054, 21103042, 21203054).

DOI: 10.1016/S1872-2067(14)60124-8 | <http://www.sciencedirect.com/science/journal/18722067> | Chin. J. Catal., Vol. 35, No. 9, September 2014

modified with Bi dopant ions [14–19]. Doping with Bi ions can decrease the band gap of TiO_2 and thereby extend its absorption into the visible light region, enhancing its photocatalytic efficiency. It has been shown that bismuth-doped TiO_2 systems are more effective for the photodegradation of organic pollutants, such as methyl orange, benzene, acetaldehyde, and isoproturon herbicide, under visible light irradiation [20–23]. Generally, in Bi-doped TiO_2 photocatalysts, the Bi-O polyhedra in bismuth titanate compounds ($\text{Bi}_x\text{Ti}_y\text{O}_z$) or the Bi^{3+} species are the active centers in the photocatalytic reaction [15,24]. Zhang et al. [25] synthesized a highly ordered mesoporous Bi-doped TiO_2 using a synchronous assembly approach. Their Bi-doped TiO_2 samples showed strong absorption in the visible light region and exhibited enhanced photocatalytic activities for phenol oxidation and chromium reduction in aqueous suspension under visible and UV light. The authors ascribed the high catalytic activity to both the unique structural characteristics of the material and the Bi doping. The high response to visible light was found to mainly originate from the doping process as a result of the formation of new Bi states in the form of Bi-O-Ti bonds and the reduction in the electron-hole recombination rate. Xu et al. [26] prepared $\text{Bi}_2\text{O}_3\text{-TiO}_2$ composite films by a sol-gel method under mild conditions. The films were composed of anatase TiO_2 and Bi_2O_3 , with the TiO_2 particles deposited on the surface of Bi_2O_3 . All of their as-prepared $\text{Bi}_2\text{O}_3\text{-TiO}_2$ composite films exhibited higher photocatalytic activity than pure TiO_2 under solar irradiation, while the film with a Bi/Ti atomic ratio of 1.25% showed the highest photocatalytic activity. Wang et al. [27] prepared bismuth- and sulfur-codoped TiO_2 by a simple sol-gel method using tetrabutyl titanate, bismuth nitrate pentahydrate, and thiourea as precursors. The codoped TiO_2 exhibited high photocatalytic activity for the photodegradation of a 20 mg/L solution of indigo carmine under visible light. The high photocatalytic performance was suggested to be associated with the existence of numerous oxygen vacancies, the acidic sites on the surface of the TiO_2 , and its high specific surface area. Zuo and co-workers [15] also prepared Bi-doped TiO_2 photocatalysts by a sol-gel process and pointed out that bismuth doping causes TiO_2 to react with Bi^{3+} ions to produce Bi_xTiO_y , which results in band-gap narrowing and a reduced threshold energy for photoactivation, potentially increasing the photoactivity.

To date, the main method used to obtain Bi-doped TiO_2 (BTO) photocatalysts has been the sol-gel approach, and there are few reports focused on the preparation of Bi-doped TiO_2 by hydrothermal methods [19]. In addition, the Ti source used is mainly tetrabutyl titanate ($\text{Ti}(\text{OC}_3\text{H}_7)_4$). In the present work, the first using nanotube titanic acid (NTA; $\text{H}_2\text{Ti}_2\text{O}_4(\text{OH})_2$) as the Ti precursor, we synthesized a series of BTO photocatalysts with different Bi/Ti molar ratios via a hydrothermal method. The as-prepared samples were characterized by X-ray diffraction (XRD), transmission electron microscopy (TEM), X-ray photoelectron spectroscopy (XPS), and ultraviolet-visible diffuse reflectance spectroscopy (UV-Vis DRS). The photocatalytic activity of the samples was evaluated for decoloration of methyl orange (MO) under visible light irradiation. For comparison, we also prepared bismuth doped TiO_2 (denoted as Bi-TiO₂)

via a sol-gel process using tetrabutyl titanate as the Ti precursor. The hydrothermally-prepared BTO system showed much higher visible-light photocatalytic activity in the photodegradation of methyl orange than that of the Bi-TiO₂ prepared by the sol-gel process. The as-fabricated BTO also showed high photoactivity for the photocatalytic degradation of 4-chlorophenol (4-CP).

2. Experimental section

2.1. Catalyst preparation

NTA was prepared using concentrated NaOH and TiO_2 as the raw materials, according to a typical previously described procedure [28,29]. In brief, 300 mL of aqueous NaOH (10 mol/L) was placed in a PTFE beaker and 3 g P25 (TiO_2) powder was added under continuous stirring. The mixture was transferred into an autoclave and heat-treated at 120 °C for 24 h. The resulting white precipitate was washed with deionized water to pH ≈ 7.0–8.0, and then immersed in HCl solution (0.1 mol/L) for 7 h under magnetic stirring. The precipitate was then washed again with deionized water to remove Cl^- , dried under vacuum at room temperature, and then ground. The product obtained was NTA.

To prepare Bi-doped TiO_2 samples using the hydrothermal method, known amounts of bismuth chloride (to give Bi/Ti molar ratios of 0%, 0.5%, 1%, 2%, and 5%) were first dissolved in 50 mL of deionized water acidified with hydrochloric acid. 1 g of as-prepared NTA was added to the solution under continuous stirring, and the resulting mixture was transferred into an autoclave and reacted at 130°C for 3 h. After cooling, the product was washed with hydrochloric acid (0.1 mol/L) and then deionized water by centrifugation. The obtained sample was dried under vacuum at room temperature and then ground. The powder samples were labeled BTO-130-0, BTO-130-0.5, BTO-130-1, BTO-130-2, and BTO-130-5, representing BTO with the above Bi/Ti molar ratios. In addition, the BTO-160-1 and BTO-210-1 samples were prepared by subjecting a Bi/Ti molar ratio = 1% precursor mixture to hydrothermal reactions at 160 and 210°C. Meanwhile, as a comparison, we also prepared bismuth doped TiO_2 (denoted as Bi-TiO₂) by a sol-gel method using tetrabutyl titanate as the Ti precursor. The Bi-TiO₂ preparation procedure was the same as that reported by Zhang et al [30]. Pure BiOCl was also synthesized using the method reported by Jiang et al [31].

2.2. Catalyst characterization

The structural properties of the as-prepared BTO samples were analyzed by XRD (Philips X'Pert Pro, Netherlands) ($\text{Cu}-K_\alpha$, $\lambda = 0.15418 \text{ nm}$ at 40 kV, 40 mA over the 2θ range 5°–90°). The morphology of the samples was observed by TEM (JEOL JEM-2010). The UV-Vis diffuse reflectance spectra (DRS) of the samples were determined using a Shimadzu U-3010 UV-Vis diffuse spectrometer equipped with an integrating sphere. A BaSO_4 standard was used as a reference sample for baseline

correction. The scan range was 200–800 nm. Binding energy was recorded by XPS with an Axis Ultra spectrometer using monochromatized Al- $K\alpha$ ($h\nu=1486.6$ eV) radiation as the excitation source. Adventitious carbon (C 1s peak at 284.8 eV) was used to calibrate the binding energy.

2.3. Photocatalytic activity

The photocatalytic activity of the BTO samples was investigated by photodegradation of methyl orange in aqueous solution under visible light irradiation. The photodegradation experiment was carried out using the following procedure: 3 mL BTO photocatalyst suspension (0.06 g/L) was placed in a quartz cell (1.0 cm × 1.0 cm × 4.5 cm) containing 50 μ L methyl orange solution (1 mmol/L) and stirred with a small magneton. A 300 W xenon lamp was used as the visible light source. The short wavelength components ($\lambda < 420$ nm) of the light were cut off using a glass optical filter. The intensity of the light with $\lambda \geq 420$ nm was estimated to be 43 mW/cm². Before irradiation, the suspension was held in the dark for 30 min to reach complete adsorption-desorption equilibrium. The MO photodegradation efficiency was monitored by detecting the change in absorbance at 464 nm between defined time intervals using the UV-Vis spectrophotometer. For comparison, the photocatalytic activity of P25 and pure BiOCl, as well as the sol-gel Bi-TiO₂ was also investigated under the same conditions as that of the BTO catalysts. The MO photodegradation rate was calculated as $(C_0 - C_t)/C_0 \times 100\%$, where C_0 and C_t represent the concentrations of the MO solution at the initial moment and time t , respectively.

3. Results and discussion

3.1. XRD analysis

The phase structure of the BTO samples was investigated by XRD, as shown in Fig. 1. The BTO-130-0, BTO-130-0.5, and BTO-130-1 samples exhibited only the characteristic peaks of anatase, and no obvious diffraction peaks corresponding to bismuth oxides were observed. However, with increase in the Bi/Ti molar ratio from 2% to 5%, a new phase assigned to BiOCl ($2\theta = 12.2^\circ, 24.2^\circ, 25.9^\circ, 32.5^\circ, 33.6^\circ, 36.9^\circ, 41.2^\circ, 46.7^\circ, 49.8^\circ$, and 58.7° , JCPDS No. 06-0249) appeared. At the same time, the anatase phase peaks gradually weakened and even disappeared (especially at Bi/Ti = 5%), which indicates that the Bi ion doping suppressed the growth of anatase TiO₂. This was caused by the newly formed BiOCl phase on the TiO₂ surface inhibiting the growth of the anatase crystals. At lower levels of Bi doping, this BiOCl phase could not be observed, which may be because the formed BiOCl content was below the detection limit of the XRD instrument. In addition, we also found that obvious diffraction peaks ascribed to BiOCl phase appeared when the hydrothermal temperature increased to 160 and 210 °C at controlled Bi/Ti molar ratio of 1%, indicating that higher hydrothermal reaction temperature promotes the generation of BiOCl phase. Based on the above XRD results, it can be concluded that Bi³⁺ was not doped into the TiO₂ lattice by replacing

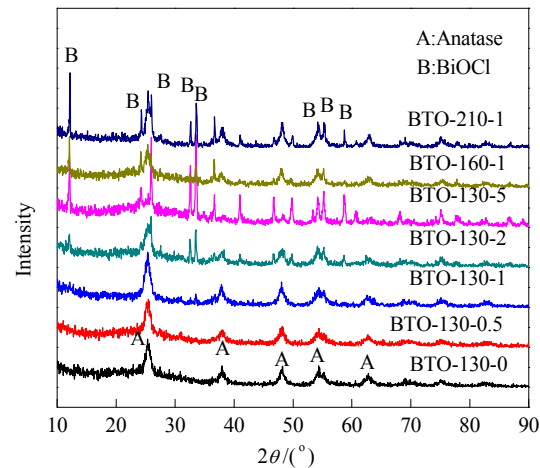


Fig. 1. XRD patterns of BTO samples.

Ti⁴⁺ ions, but instead existed in the form of BiOCl on the TiO₂ surface.

3.2. Surface morphology of the photocatalysts

TEM images of the BTO samples are displayed in Fig. 2. Almost all of the samples exhibited diamond schistose-like structure with an average size of 10–20 nm, which did not change with the increase in Bi/Ti molar ratio. Zheng et al. [32] reported that the morphology of TiO₂ crystalline grains was associated with the type of precursor used and the acidity or basicity of the hydrothermal reaction medium. They also pointed out that, under acidic conditions, the product of the hydrothermal reaction was anatase phase TiO₂ with diamond schistose-like structure, similar to that obtained herein.

3.3. XPS study

Figure 3 shows the high-resolution XPS spectra of the BTO samples. From Fig. 3(a), we can see that two peaks, assigned to Ti 2p_{3/2} and Ti 2p_{1/2}, existed in the Ti 2p spin-orbital spectrum. The Ti 2p_{3/2} and 2p_{1/2} peaks were located at binding energy of about 458.8 and 464.6 eV, respectively, which correspond to a + 4 valence state of the Ti cations in TiO₂ [33,34]. The Bi 4f XPS line (Fig. 3(b)) shows peaks centered at 164.6 and 159.0 eV corresponding to the binding energy of Bi 4f_{7/2} and Bi 4f_{5/2}, respectively, indicating that the main chemical state of bismuth in the samples was trivalence [35]. From Fig. 3(c), it can be seen that the O 1s peak could be divided into two different peaks at 529.4 and 530.8 eV. The former is attributed to the Ti-O bond in the TiO₂ crystal lattice, while the latter is lower than 531.5 eV of O-H resulting from chemisorbed water [36]. The peak at 530.8 eV may originate from Bi-O [37]. From Fig. 3(d), two weak peaks around at 198.0 and 199.6 eV can be seen for all samples, which should be ascribed to Cl 2p_{3/2} and Cl 2p_{1/2} [37,38], respectively. This further demonstrates the presence of BiOCl phase, in accordance with the XRD results.

3.4. Optical absorption of BTO photocatalysts

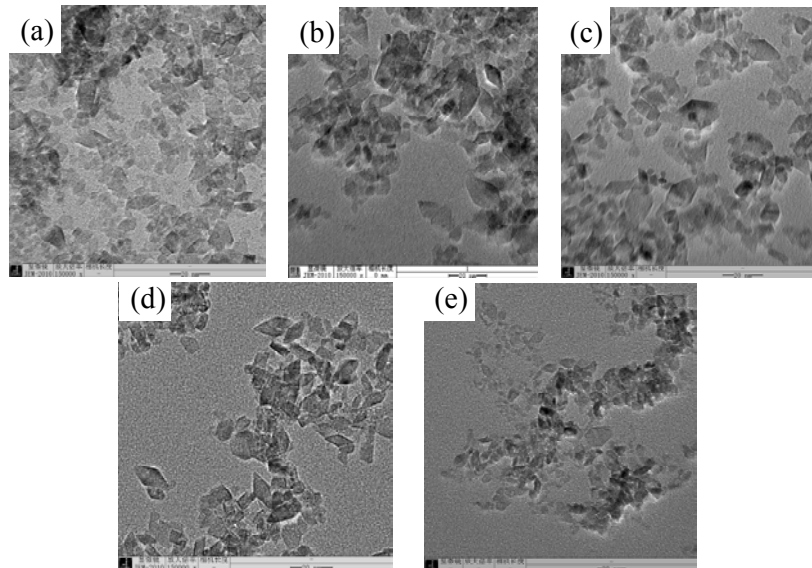


Fig. 2. TEM images of the BTO samples. (a) BTO-130-0; (b) BTO-130-0.5; (c) BTO-130-1; (d) BTO-130-2; (e) BTO-130-5.

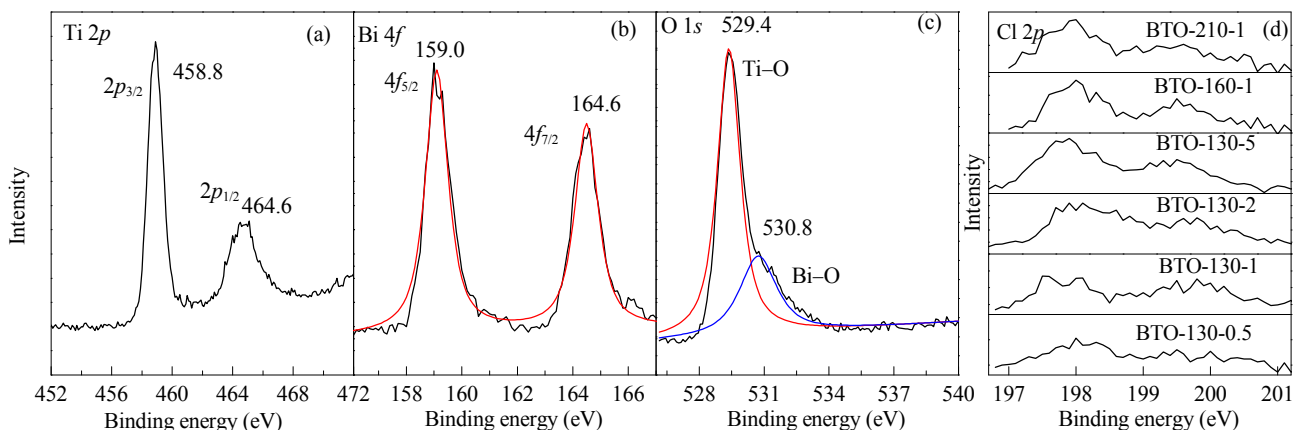


Fig. 3. High-resolution XPS spectra of BTO samples. (a) Ti 2p of BTO-130-1; (b) Bi 4f of BTO-130-1; (c) O 1s of BTO-130-1; (d) Cl 2p of BTO samples.

The UV-Vis DRS spectra of the BTO samples were investigated to elucidate the effect of Bi-doping on the optical properties of the TiO_2 , and the results are shown in Fig. 4. The DRS spectrum of P25 is also given for comparison. From Fig. 4(a), it can be seen that the bismuth doping did affect the light absorption property of the catalysts. Compared with that of P25, the photo-absorption of the BTO samples obtained after hydrothermal treatment at 130 °C for 3 h exhibited a red shift towards the visible light region to some extent. As expected, the degree of red shift differed with the Bi/Ti molar ratio. According to the XRD and XPS analysis results, the Bi^{3+} did not incorporate into the TiO_2 lattice, and were present in the form of BiOCl phase. Therefore, we should call our BTO as BiOCl composites TiO_2 . However, BiOCl , a new type of photocatalyst with a band gap of 3.2 eV, only exhibits strong absorption in the ultraviolet region [39]. Our previous studies have indicated that hydrothermal treatment of NTA generates large amounts of single-electron-trapped oxygen vacancies (SETOVs). These SETOVs form an intra-band level below the conduction band, which contributes to visible light absorption [40–42]. So, we can ascribe the visible-light absorption of the BiOCl composites

TiO_2 catalysts in the present work to the formation of SETOVs during the process of NTA hydrothermal treatment. Fig. 4(b) shows the effect of hydrothermal reaction temperature on the absorption of the BiOCl composites samples. It can be seen that the visible light absorption intensity of these samples was similar despite the increase in reaction temperature, which is in agreement with reports from the literature [40].

3.5. Photocatalytic activity

The photocatalytic activity of the BTO catalysts was studied by photodegradation of MO in aqueous solution under visible light irradiation. Figure 5 displays the degradation efficiency of MO over different photocatalyst samples under visible light irradiation. MO was very stable in the absence of light or a photocatalyst. The comparison photocatalysts P25 and pure BiOCl showed slight photocatalytic activity for the degradation of MO (Fig. 5(a)), which is possible because a small amount of ultraviolet light is remained in the light source. Upon introducing Bi ions into the TiO_2 system, all the composites samples showed high photoactivity for the photodegradation of MO

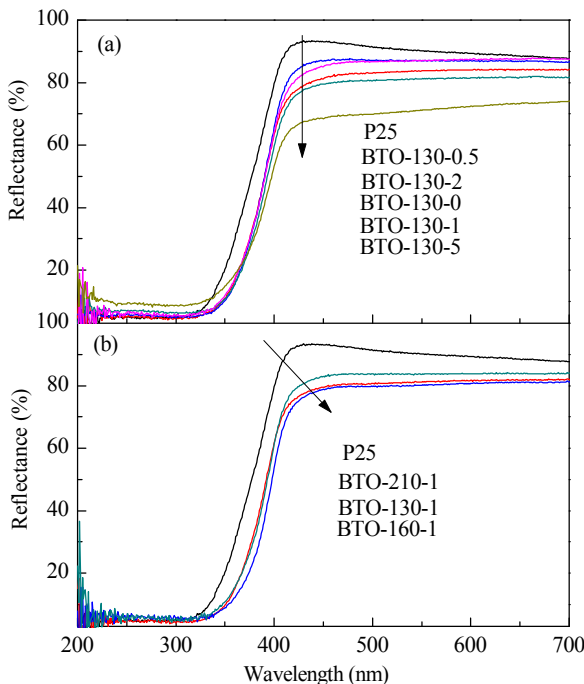


Fig. 4. UV-Vis DRS spectra of P25 and BTO samples.

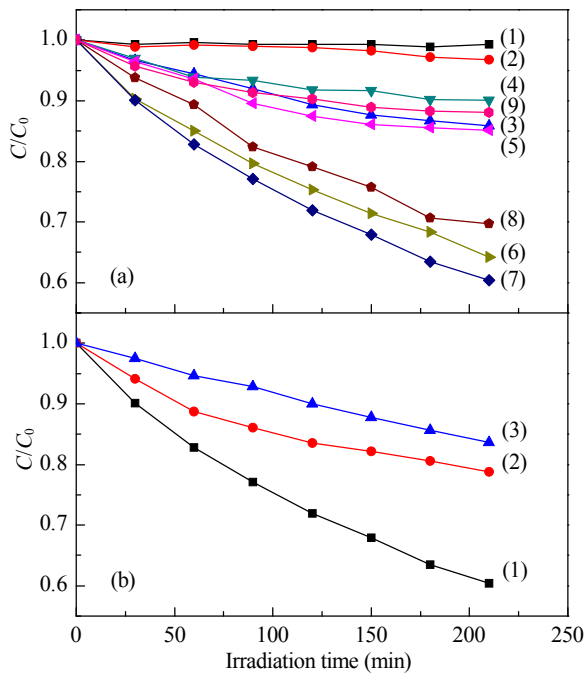


Fig. 5. Degradation of MO over different catalysts under visible light irradiation. (a): (1) Without irradiation; (2) Without catalyst; (3) P25; (4) Pure BiOCl; (5) BTO-130-0; (6) BTO-130-0.5; (7) BTO-130-1; (8) BTO-130-2; (9) BTO-130-5. (b): (1) BTO-130-1; (2) BTO-160-1; (3) BTO-210-1.

except for Bi/Ti molar ratio = 5%. The photocatalytic activity of the BTO samples increased rapidly with Bi dopant level, and reached a maximum value at Bi/Ti molar ratio = 1%. In contrast, as the Bi dopant level was increased to 5%, the photocatalytic activity gradually decreased and was finally reduced to a level lower than that of P25. The effect of the hydrothermal reaction temperature on the photocatalytic activity was also

studied. At Bi/Ti molar ratio = 1%, the photocatalytic activity decreased when the hydrothermal reaction temperature was increased above 130 °C (Fig. 5(b)). Thus, it can be concluded that the optimal Bi/Ti molar ratio is 1% and the optimal hydrothermal temperature is 130 °C.

Figure 6 shows the photodegradation kinetics of MO over P25 and the BTO samples. In the studied concentration range, the photocatalytic degradation appears to follow pseudo first-order reaction kinetics, which can be expressed as follows:

$$\ln(C_0/C_t) = k_{app} \times t,$$

where k_{app} is the apparent first-order reaction rate constant, used as the basic kinetic parameter for the different photocatalysts because it allows the photocatalytic activity to be determined independent of the adsorption period in the dark and the concentration of MO remaining in the solution. From Fig. 6, it can be seen that the BTO photocatalysts had obviously increased apparent first-order rate constants for the photocatalytic degradation of MO under visible light irradiation. The apparent rate constants (or the photocatalytic activity) followed the following trend: BTO-130-1 > BTO-130-0.5 > BTO-130-2 > BTO-130-0 > P25 > BTO-130-5. Namely, the rate constant of the composited TiO₂ samples first increased with Bi/Ti molar ratio and reached a maximum at Bi/Ti molar ratio = 1%, i.e., for the BTO-130-1 sample. At higher Bi ion doping levels, the rate constant of the samples decreased, eventually dropped to a level similar to that of P25, and for the sample BTO-130-5, even lower than that of P25. These results imply that an excess of Bi ions led to a decrease in the photodegradation efficiency of MO, which may have resulted from the generation of excess BiOCl phase. The XRD and XPS results demonstrate that Bi³⁺ did not incorporate into the lattice of TiO₂, and were instead present in the form of BiOCl phase. In addition, higher Bi doping level and hydrothermal temperature promoted the formation of BiOCl phase, meaning the generation of greater amounts of BiOCl phase. The deposition of more BiOCl phase on the TiO₂ surface would hinder the transfer of photogenerated electrons and holes to the surface, and too much BiOCl would form recombi-

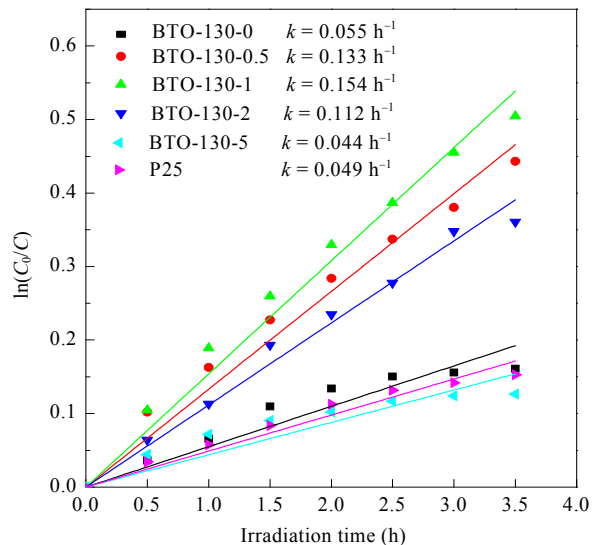


Fig. 6. First order kinetic curves of MO degradation over different photocatalysts.

nation centers where photo-induced carriers could be captured, thereby leading to lower photocatalytic activity [43]. Both undoped-TiO₂ and pure BiOCl exhibited very low photocatalytic activity under visible light irradiation, as shown in Fig. 5. However, when the Bi/Ti molar ratio = 0.5% and 1%, the formed BiOCl/TiO₂ composite showed higher activity than undoped-TiO₂ and pure BiOCl, which may have originated from the different energy band positions of these two semiconductors. According to literature [39,44], the valence band and conduction band positions of BiOCl are lower than those of TiO₂. This difference in energy band position accelerated the transfer and separation of photogenerated carriers [45], and further enhanced the photocatalytic activity. This is mainly because the generation of BiOCl may introduce lattice defects in TiO₂ and produce more photocatalytically active sites, as discussed in the photocatalytic mechanism section below.

In the present work, we also introduced bismuth ions into a TiO₂ system (the obtained sample was denoted Bi-TiO₂) using a sol-gel method with tetrabutyl titanate as the Ti precursor (Bi/Ti = 1%), and compared its photocatalytic activity with that of the corresponding hydrothermally-prepared BiOCl/TiO₂ composite (Fig. 7). Hydrothermal synthesis is a well-known technique that can be used to prepare metal ion-doped oxides in a sealed high-temperature and high-pressure environment [46]. Differing from the conventional sol-gel methods, hydrothermal methods can offer many advantages, such as energy conservation, simple preparation, rapid reaction, and low operation temperature. This is evidenced by the decreased visible light photocatalytic activity of Bi-TiO₂ sample. As shown in Fig. 7, the hydrothermally-obtained photocatalyst composite displayed much higher photocatalytic activity than the Bi-TiO₂ catalyst.

The photocatalytic degradation of 4-chlorophenol was also investigated over the BTO sample. Herein, we only chose BTO-130-1 sample. The result is shown in Fig. 8. The photo-degradation of 4-chlorophenol was carried out in a 100 mL photocatalytic reactor system by adding 0.1 g catalyst into 4-chlorophenol solution of an initial concentration of 12 mg/L. Prior to illumination, the mixture of photocatalyst and 4-chlorophenol solution was kept in the dark for 2 h to estab-

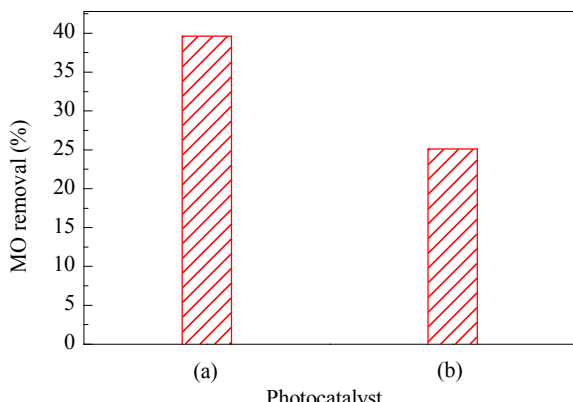


Fig. 7. Comparison of the efficiency of MO photodegradation over BTO-130-1 obtained by hydrothermal method (a) and Bi-TiO₂ with Bi/Ti molar ratio = 1% obtained by sol-gel method (b).

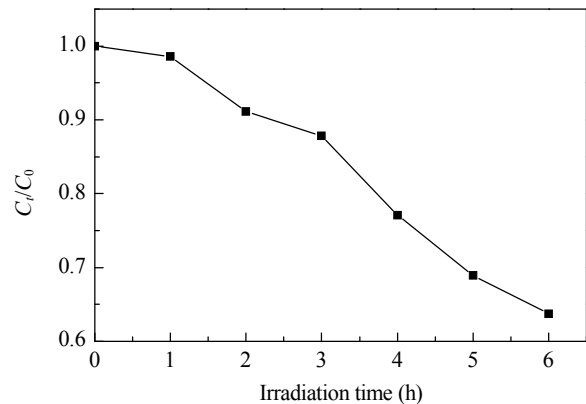


Fig. 8. Degradation of 4-chlorophenol over the BTO-130-1 sample under visible light irradiation.

lish adsorption-desorption equilibrium. The visible light irradiation time was 6 h, and samples for analysis were taken from the suspension at 1 h intervals and immediately centrifuged. The photocatalytic activity was evaluated by monitoring the change in absorbance of the 4-chlorophenol solution at a wavelength of 227 nm. The absorbance decreased obviously after visible light irradiation for 6 h, implying that the obtained BTO photocatalyst showed high photoactivity for the photo-degradation of organic pollutant 4-chlorophenol.

3.6. Mechanism of the photocatalytic degradation of MO on BTO samples

On the basis of the above analysis, the high photocatalytic activity possessed by the present BTO catalysts can be ascribed to the formation of SETOVs in the TiO₂ matrix during the hydrothermal treatment of NTA and the generation of the composite. The formed SETOVs extended the absorption of the TiO₂ into the visible light region, while the generation of the BiOCl/TiO₂ composite improved the transfer and separation of photo-induced carriers. The synergistic effect between the two facilitated the enhancement of the photocatalytic activity of the catalyst. It has been reported that the valence band (VB) and conduction band (CB) edge potentials of BiOCl, which has a band-gap energy of 3.2 eV, are 3.44 and 0.24 eV, respectively [39], which means that the VB and CB levels of BiOCl are lower than those of TiO₂ [44]. Thus, we propose a possible photocatalytic mechanism for the degradation of MO on the composited photocatalysts. To explain the mechanism of the photocatalytic degradation, we examined the active species by observing the degradation yield of MO obtained after adding different types of active species scavengers. The results obtained under different conditions are compared in Fig. 9. Obvious decreases in the MO removal rate were observed upon adding methanol to capture photogenerated holes, upon adding benzoquinone to capture O₂• radicals, and upon adding terephthalic acid to capture OH• radicals. However, an abrupt increase in the photodegradation of MO was observed when silver nitrate was added to the reaction system to capture photogenerated electrons. This demonstrated that, except for photogener-

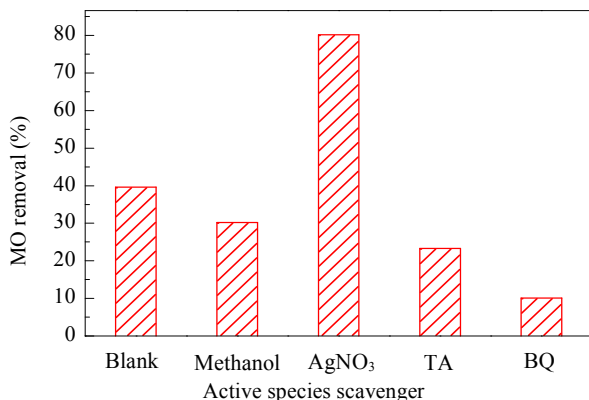


Fig. 9. Comparison of MO photodegradation efficiency over BTO-130-1 after adding different active species scavengers. TA and BQ represent terephthalic acid and benzoquinone, respectively.

ated electrons, both $\text{O}_2^{\cdot-}$ radicals and OH^{\cdot} radicals as well as photogenerated holes were the active species in the process of MO degradation over the present catalysts. The corresponding reaction mechanism is described in Fig. 10. Under visible light irradiation, the electrons from the VB of TiO_2 are first excited to the intra-band contributed by the SETOVs and are trapped by the SETOVs. Subsequently, the trapped electrons can be further excited to the CB of TiO_2 by visible light. These electrons can be transferred from the CB of TiO_2 to CB of BiOCl . This process results in more effective separation of photogenerated electron-hole pairs and faster interfacial charge transfer than in a mono-semiconductor, and the recombination of the excited electrons and holes is effectively inhibited. The excited electrons and transferred electrons can be trapped by surface absorbed molecular oxygen (O_2) to form superoxide anion radicals ($\text{O}_2^{\cdot-}$). Meanwhile, the photogenerated holes in the VB can be trapped by OH^- or H_2O species adsorbed on the catalyst surface to generate reactive hydroxyl radicals (OH^{\cdot}) in aqueous media. These two radicals are powerful oxidizing agents capable of degrading organic compounds. Photogenerated holes possessing powerful oxidizing ability can directly oxidize MO, leading to its decomposition. As a result, the BTO system exhibited high photocatalytic activity for MO photodegradation under visible light irradiation.

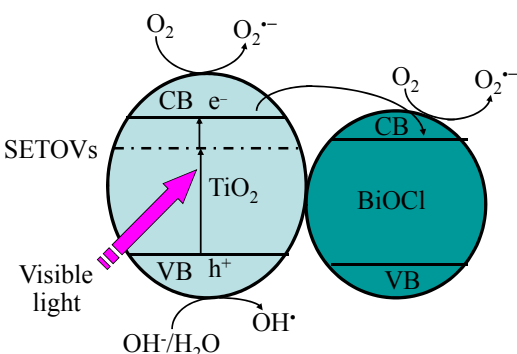


Fig. 10. Schematic of mechanism for MO degradation over BTO samples under visible light irradiation.

4. Conclusions

A series of BTO photocatalysts with different Bi/Ti molar ratios have been synthesized by a hydrothermal method using NTA as the Ti precursor. The results show that the Bi ions do not incorporate into the TiO_2 lattice but instead mainly exist in the form of BiOCl phase near the TiO_2 surface, forming a $\text{BiOCl}/\text{TiO}_2$ composite. The obtained products possess a rhombus schistose-like anatase structure. The visible light photocatalytic degradation of methyl orange over the composited TiO_2 samples demonstrates that they have higher photodegradation activity than that of P25. The high photocatalytic activity is attributed to both the presence of SETOVs and the formation of $\text{BiOCl}/\text{TiO}_2$ composite. The formation of SETOVs in the TiO_2 matrix during the process of NTA hydrothermal treatment results in visible light sensitization, while the formed $\text{BiOCl}/\text{TiO}_2$ composite improves the separation of photogenerated electrons and holes and prevents them from recombining. In addition, the as-prepared photocatalyst composite also shows high photocatalytic activity for the photodegradation of 4-chlorophenol.

References

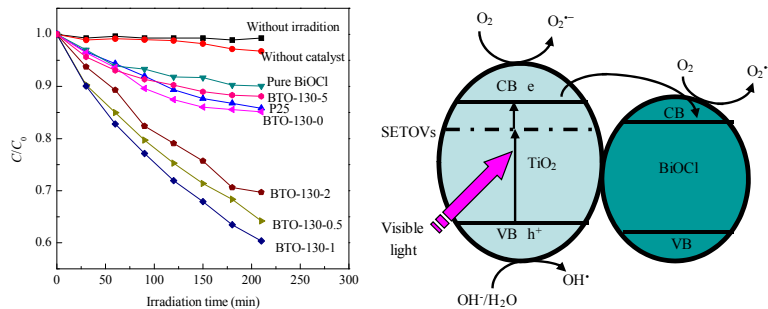
- [1] Yang C C, Yu Y H, van der Linden B, Wu J C S, Mul G. *J Am Chem Soc*, 2010, 132: 8398
- [2] Hoffmann M R, Martin S T, Choi W Y, Bahnemann D W. *Chem Rev*, 1995, 95: 69
- [3] Fujishima A, Honda K. *Nature*, 1972, 238: 37
- [4] Fujishima A, Rao T N, Tryk D A. *J Photochem Photobiol C*, 2000, 1: 1
- [5] Wu Q P, Zheng Q, van de Krol R. *J Phys Chem C*, 2012, 116: 7219
- [6] Tian B Z, Li C Z, Gu F, Jiang H B, Hu Y J, Zhang J L. *Chem Eng J*, 2009, 151: 220
- [7] Chang J S, Hwang Y K, Ariga K. *J Nanosci Nanotechnol*, 2010, 10: 1
- [8] Asahi R, Morikawa T, Ohwaki T, Aoki K, Taga Y. *Science*, 2001, 293: 269
- [9] Ren W J, Ai Z H, Jia F L, Zhang L Z, Fan X X, Zou Z G. *Appl Catal B*, 2007, 69: 138
- [10] Liu G, Zhao Y N, Sun C H, Li F, Lu G Q, Cheng H M. *Angew Chem Int Ed*, 2008, 47: 4516
- [11] Choi W Y, Termin A, Hoffmann M R. *J Phys Chem*, 1994, 98: 13669
- [12] Štengl V, Bakardjieva S, Murafa N. *Mater Chem Phys*, 2009, 114: 217
- [13] Xu A W, Gao Y, Liu H Q. *J Catal*, 2002, 207: 151
- [14] Xu J J, Chen M D, Fu D G. *Appl Surf Sci*, 2011, 257: 7381
- [15] Zuo H S, Sun J, Deng K J, Su R, Wei F Y, Wang D Y. *Chem Eng Technol*, 2007, 30: 577
- [16] Murcia-López S, Hidalgo M C, Navío J A. *Appl Catal A*, 2011, 404: 59
- [17] Hu Y, Cao Y T, Wang P X, Li D Z, Chen W, He Y H, Fu X Z, Shao Y, Zheng Y. *Appl Catal B*, 2012, 125: 294
- [18] Li H Y, Wang D J, Wang P, Fan H M, Xie T F. *Chem Eur J*, 2009, 15: 12521
- [19] Ji T H, Yang F, Lü Y Y, Zhou J Y, Sun J Y. *Mater Lett*, 2009, 63: 2044
- [20] Yu J X, Liu S W, Xiu Z L, Yu W N, Feng G J. *J Alloys Compd*, 2008, 461: L17
- [21] Hong W J, Kang M. *Mater Lett*, 2006, 60: 1296
- [22] Kang M, Ko Y R, Jeon M K, Lee S C, Choung S J, Park J Y, Kim S, Choi S H. *J Photochem Photobiol A*, 2005, 173: 128
- [23] Reddy P A K, Srinivas B, Kala P, Kumari V D, Subrahmanyam M. *Mater Res Bull*, 2011, 46: 1766

Graphical Abstract

Chin. J. Catal., 2014, 35: 1578–1589 doi: 10.1016/S1872-2067(14)60124-8

Preparation of Bi-doped TiO₂ nanoparticles and their visible light photocatalytic performance

Haiyan Li, Jinfeng Liu, Junjie Qian, Qiuye Li, Jianjun Yang*
Henan University



Bi-doped TiO₂ photocatalysts showed high visible light photocatalytic activity for the degradation of methyl orange and 4-chlorophenol. The high photoactivity was co-determined by single-electron-trapped oxygen vacancies (SETOVs) and the formation of a BiOCl/TiO₂ composite. The formation of SETOVs during the process of NTA hydrothermal treatment accounts for the visible light sensitization, while the formed BiOCl/TiO₂ composite improves the separation of photogenerated electrons and holes and prevents them from recombining.

- [24] Yao W F, Wang H, Xu X H, Cheng X F, Huang J, Shang S X, Yang X N, Wang M. *Appl Catal A*, 2003, 243: 185
- [25] Sajjad S, Leghari S A K, Chen F, Zhang J L. *Chem Eur J*, 2010, 16: 13795
- [26] Xu J J, Ao Y H, Fu D G, Yuan C W. *Appl Surf Sci*, 2008, 255: 2365
- [27] Wang Y, Wang Y, Meng Y L, Ding H M, Shan Y K, Zhao X, Tang X Z. *J Phys Chem C*, 2008, 112: 6620
- [28] Zhang S L, Zhou J F, Zhang Z J, Du Z L, Vorontsov A V, Jin Z S. *Chin Sci Bull* (张顺利, 周静芳, 张治军, 杜祖亮, Vorontsov A V, 金振声, 科学通报), 2000, 45: 1104
- [29] Yang J J, Jin Z S, Wang X D, Li W, Zhang J W, Zhang S L, Guo X Y, Zhang Z J. *Dalton Trans*, 2003: 3898
- [30] Zhang M, Feng C X, Jin Z S, Cheng G, Du Z L, Dang H X. *Chin J Catal* (张敏, 冯彩霞, 金振声, 程刚, 杜祖亮, 邓鸿辛. 催化学报), 2005, 26: 508
- [31] Jiang J, Zhao K, Xiao X Y, Zhang L Z. *J Am Chem Soc*, 2012, 134: 4473
- [32] Zheng Y Q, Shi E W, Yuan R L, Li W J, Wang B G, Zhong W Z, Hu X F. *Sci China (Series E)* (郑燕青, 施尔畏, 元如林, 李汶军, 王步国, 仲维卓, 胡行方. 中国科学E辑), 1999, 29: 206
- [33] Shi L Y, Gu H C, Li C Z, Fang D Y, Zhang Y, Hua B. *Chin J Catal* (施利毅, 古宏晨, 李春忠, 房鼎业, 张怡, 华彬. 催化学报), 1999, 20: 338
- [34] Lü K L, Zuo H S, Sun J, Deng K J, Liu S C, Li X F, Wang D Y. *J Hazard Mater*, 2009, 161: 396
- [35] Morgan W E, Stec W J, Van Wazer J R. *Inorg Chem*, 1973, 12: 953
- [36] Wang J, Jing L Q, Xue L P, Qu Y C, Fu H G. *J Hazard Mater*, 2008, 160: 208
- [37] Yu Z Y, Detlef B, Ralf D, Song L, Lu L Q. *J Mol Catal A*, 2012, 365: 1
- [38] Cao J, Xu B Y, Lin H L, Luo B D, Chen S F. *Catal Commun*, 2012, 26: 204
- [39] Zhang W D, Zhang Q, Dong F. *Ind Eng Chem Res*, 2013, 52: 6740
- [40] Cui G J, Xu Z X, Wang Y, Zhang M, Yang J J. *Surf Rev Lett*, 2008, 15: 509
- [41] Wang Y, Feng C X, Zhang M, Yang J J, Zhang Z J. *Appl Catal B*, 2011, 104: 268
- [42] Yu X L, Wang Y, Meng X J, Yang J J. *Chin J Catal* (于新奕, 王岩, 孟祥江, 杨建军. 催化学报), 2013, 34: 1418
- [43] Leng W H, Cheng S A, Liu H, Zhang J Q, Cao C N. *Acta Sci Circum* (冷文华, 成少安, 刘鸿, 张鉴清, 曹楚南. 环境科学学报), 2000, 20: 499
- [44] Tong H, Ouyang S X, Bi Y P, Umezawa N, Oshikiri M, Ye J H. *Adv Mater*, 2012, 24: 229
- [45] Chen H J, Yin G J, Wu C L. *Chin J Environ Eng* (陈华军, 尹国杰, 吴春来. 环境工程学报), 2008, 2: 1516
- [46] Jiao Y C, Zhu M F, Chen F, Zhang J L. *Chin J Catal* (焦艳超, 朱明峰, 陈锋, 张金龙. 催化学报), 2013, 34: 585

铋掺杂二氧化钛纳米颗粒的制备及其可见光催化性能

李海燕^{a,b}, 刘金凤^a, 钱俊杰^a, 李秋叶^a, 杨建军^{a,*}

^a河南大学特种功能材料重点实验室, 河南开封475004

^b河南大学化学化工学院, 河南开封475004

摘要: 采用水热法, 以纳米管钛酸为前驱物制备了Bi掺杂的TiO₂, 并利用X射线衍射、透射电子显微镜、X射线光电子能谱、紫外-可见漫反射光谱等手段对样品进行了表征。以甲基橙的光催化降解为模型反应评价了样品的可见光催化性能。结果表明, Bi离子并没有进入TiO₂的晶格中, 而是以BiOCl的形式存在。所制得的BiOCl/TiO₂复合物对甲基橙降解表现出较优越的可见光催化活性; 当Bi/Ti摩尔比为1%, 水热温度为130°C时, 所制催化剂的光催化性能最佳, 并对光催化活性提高的机理进行了讨论。同时, 该催化

剂对4-氯苯酚降解也表现出较高的光催化性能。

关键词: 水热法; 钇掺杂; 二氧化钛; 纳米管钛酸; 氧空位; 可见光催化

收稿日期: 2014-02-24. 接受日期: 2014-04-21. 出版日期: 2014-09-20.

*通讯联系人。电话/传真: (0371)23881358; 电子信箱: yangjianjun@henu.edu.cn

基金来源: 国家自然科学基金(20973054, 21103042, 21203054).

本文的英文电子版由Elsevier出版社在ScienceDirect上出版(<http://www.sciencedirect.com/science/journal/18722067>).

1. 前言

作为一种具有潜力的光催化剂半导体, TiO_2 因具有生物和化学惰性、耐光腐蚀和化学腐蚀、无毒、廉价等优点, 已被广泛应用于空气的净化, 水的纯化以及光催化分解水等^[1–3]. TiO_2 对有机污染物的光催化氧化通常表现出较高的活性^[4], 然而对太阳光较低的利用率(只能利用紫外光)以及较高的电子-空穴复合率限制了 TiO_2 的实际应用. 为了提高 TiO_2 对太阳光谱的利用以及抑制光生电子-空穴对的复合, 一个主要的方法就是用过渡金属(比如Fe, V, Cr等)^[5–7]或者非金属元素(比如N, C, B等)^[8–10]对其进行掺杂. 金属离子掺杂的 TiO_2 已被广泛研究, 不仅可将 TiO_2 的吸收扩展至可见光区, 而且合适的金属离子的掺杂量能够抑制电子-空穴的复合^[11]. 确实, 各种金属离子的掺杂促进了光催化性能的提高以及对可见光的响应^[12,13]. 在掺杂体系中, 掺杂的金属离子可能作为电子或空穴的捕获阱, 从而改变电子-空穴的复合速率; 此外, 金属元素的掺杂对带隙的窄化也是有利的.

最近, 用Bi离子对 TiO_2 掺杂改性引起了人们广泛的关注^[14–19]. 用Bi离子进行掺杂可以降低 TiO_2 的带隙, 将其吸收光谱扩展至可见光区, 从而提高其光催化效率. Bi掺杂的 TiO_2 在可见光下降解有机污染物(比如甲基橙、苯、乙醛、除草剂异丙隆等^[20–23])中表现出优异的性能. 通常, 在Bi掺杂的 TiO_2 光催化剂中, 钛酸铋复合物($Bi_xTi_yO_z$)中的Bi-O多面体以及Bi³⁺物种是光催化反应中的活性中心^[15,24]. Zhang课题组^[25]通过使用一种共组装法合成了高度有序的介孔Bi掺杂 TiO_2 , 其在可见光区表现出了强烈的吸收, 并对可见光和紫外光下苯酚的氧化以及铬的还原表现出增强的光催化活性. 他们将表现出的高催化活性归因于这种材料独特的结构特征及Bi的掺杂; 同时对可见光的响应主要源于掺杂过程中形成的Bi-O-Ti键以及电子-空穴复合率的降低. Xu等^[26]通过在温和的条件下使用溶胶-凝胶法合成了 Bi_2O_3 - TiO_2 复合薄膜. 该薄膜主要由锐钛矿相 TiO_2 和 Bi_2O_3 构成, 且 TiO_2 颗粒沉积在 Bi_2O_3 表面上. 在太阳光照射下, 相对于纯 TiO_2 , 所有 Bi_2O_3 - TiO_2 复合薄膜均表现出较高的光催

化活性, 且当Bi含量为1.25%时, 光催化性能最佳. Wang等^[27]采用溶胶-凝胶法以钛酸四丁酯, 五水硝酸铋和硫脲为前驱体制备了Bi和S共掺杂的 TiO_2 , 共掺杂 TiO_2 对可见光下20 mg/L的食用靛蓝溶液的降解表现出较高的光催化活性. 他们将其优越的光催化性能归因于氧空位和 TiO_2 表面酸性位的存在以及较大的比表面积. Zuo等^[15]利用溶胶-凝胶法也制备了Bi掺杂的 TiO_2 , 并且指出Bi的掺杂引起 TiO_2 和Bi离子的反应, 形成 Bi_xTiO_y , 导致了带隙窄化, 降低了光反应的能量, 促进了光活性的提高.

基于上述文献, 可以看出Bi掺杂的 TiO_2 确实是一种有潜力的可见光催化剂. 到目前为止, 获得Bi掺杂 TiO_2 光催化剂的方法主要是溶胶-凝胶法. 有关水热法制备Bi掺杂 TiO_2 的报道非常少^[19]. 此外, 样品制备过程中的Ti源主要是钛酸四丁酯. 在本文中, 首次使用纳米管钛酸(NTA; $H_2Ti_2O_4(OH)_2$)作为Ti的前驱物, 采用水热法合成了一系列具有不同Bi/Ti摩尔比的BTO光催化剂. 并用XRD, TEM, XPS和UV-Vis DRS对样品进行了表征. 光催化活性通过甲基橙(MO)在可见光下的脱色进行评价. 为了比较, 本文也使用钛酸四丁酯为Ti源, 采用溶胶-凝胶法制备了Bi掺杂的 TiO_2 (标记为Bi- TiO_2).

2. 实验部分

2.1. 催化剂的制备

以NaOH和 TiO_2 为原料, 参照文献[28,29]制备NTA. 在聚四氟乙烯烧杯中配制300 ml的NaOH溶液(10 mol/L)并冷却至室温. 然后, 在不断搅拌下加入3 g P25- TiO_2 粉末. 所得混合物转移至高压反应釜中并于120 °C热处理24 h, 得到的白色沉淀用去离子水洗涤至pH = 7.0–8.0, 然后用HCl溶液(0.1 mol/L)在磁力搅拌下浸泡7 h. 随后, 将所得产物再次用去离子水洗涤以除去 Cl^- , 室温真空干燥, 研磨, 所得产物即为NTA.

Bi掺杂的 TiO_2 样品采用水热法制备. 将已知量的 $BiCl_3$ 溶解在50 ml的HCl酸化的去离子水中. 然后, 在不断搅拌下向该溶液中加入1 g新制备的NTA(Bi/Ti摩尔比为0%, 0.5%, 1%, 2%, 5%), 将混合物转移至高压反应釜

中于130 °C反应3 h。所得产品通过离心的方式依次用HCl(0.1 mol/L)和去离子水洗涤。所得样品于室温真空干燥,研磨,根据上述Bi/Ti摩尔比依次标记为BTO-130-0, BTO-130-0.5, BTO-130-1, BTO-130-2 和 BTO-130-5。然后控制Bi/Ti摩尔比为1%并调整水热反应温度为160和210 °C,所得样品分别标记为BTO-160-1和BTO-210-1。同时,作为比较,以钛酸四丁酯作为Ti源,也采用溶胶-凝胶法制备Bi掺杂的TiO₂(标记为Bi-TiO₂)。Bi-TiO₂的制备过程根据Zhang等^[30]的方法。根据Jiang等^[31]的方法,合成纯BiOCl。

2.2. 催化剂的表征

Bi掺杂TiO₂样品的结构特征采用荷兰Philips X’Pert Pro型X射线粉末衍射仪(XRD)进行分析,Cu-K_α辐射,λ=0.15418 nm,工作电压40 kV,电流40 mA,扫描范围2θ=5°–90°。样品的形貌使用JEOL JEM-2010型透射电镜(TEM)进行测定。样品的紫外-可见漫反射光谱(UV-Vis DRS)使用配备积分球的日本岛津U-3010紫外-可见漫反射谱仪进行测试,以硫酸钡为参比,扫描范围为200–800 nm。Bi的掺杂形式采用Axis Ultra型X射线光电子能谱(XPS)表征,采用单色化的Al靶(Al-K_α, hν = 1486.6 eV)为射线源。用污染C(C1s: 284.8 eV)进行能带校正。

2.3. 光催化活性

Bi掺杂TiO₂样品的光催化活性通过可见光下甲基橙溶液的光降解进行评价。光降解实验按照下面的过程进行:移取3 mL Bi掺杂TiO₂光催化剂悬浊液(0.06 g/L)加入到含有50 μL甲基橙溶液(1 mmol/L)的比色皿(1.0 cm × 1.0 cm × 4.5 cm)中,使用磁子进行搅拌。光源为300 W的氙灯。采用一个玻璃光学滤光片滤掉短波长部分的光(λ < 420 nm),得到光强为43 mW/cm²的可见光(λ ≥ 420 nm)。光照之前,首先于暗态维持30 min以达到完全的吸附-脱附平衡。甲基橙的光降解效率通过在固定的时间间隔内采用紫外-可见分光光度计测定其在λ=464 nm处吸光度的变化进行衡量。为了比较,P25-TiO₂和纯BiOCl以及溶胶-凝胶法制备的Bi掺杂TiO₂的光催化活性也在同样的条件下进行测试。甲基橙的光降解率=(C₀ - C_t)/C₀ × 100%。式中C₀和C_t分别为MO溶液的初始浓度和光照t时刻的浓度。

3. 结果与讨论

3.1. XRD结果

Bi掺杂TiO₂样品的XRD谱如图1所示。可以看出,样品BTO-130-0, BTO-130-0.5和BTO-130-1仅出现锐钛

矿相的特征峰,没有明显的铋氧化物的衍射峰。然而,伴随着Bi/Ti摩尔比从2%增加至5%,出现了BiOCl的新相,其衍射峰位于2θ=12.2°, 24.2°, 25.9°, 32.5°, 33.6°, 36.9°, 41.2°, 46.7°, 49.8°和58.7°,对应于标准卡06-0249。同时锐钛矿相的峰逐渐变弱甚至消失(尤其是在Bi/Ti摩尔比=5%时),表明Bi离子的掺杂抑制了锐钛矿相TiO₂的生长。这是由于新形成的BiOCl相位于TiO₂的表面上,抑制了锐钛矿相晶粒的生长。Bi掺杂量较低时,没有发现BiOCl相产生,这可能是由于形成的BiOCl的量低于XRD仪器的检测限。此外,我们发现当控制Bi/Ti摩尔比=1%,水热反应温度增加至160和210 °C时,也出现明显的BiOCl相衍射峰,这表明较高的水热反应温度促进了BiOCl相的形成。根据XRD分析结果,可以得出结论: Bi离子并没有掺入到TiO₂的晶格中取代Ti离子,而是以BiOCl的形式存在于TiO₂的表面。

3.2. 光催化剂的表面形貌

图2为Bi掺杂TiO₂样品的TEM照片。可以看出,几乎所有的Bi掺杂样品都表现出菱形片状结构,且不会随着Bi/Ti摩尔比的增加而变化,颗粒的平均尺寸为10–20 nm。Zheng等^[32]曾报道TiO₂晶粒的形貌与前驱物的种类及水热反应介质的酸碱度有关;在酸性条件下水热反应的产物是菱形片状结构的锐钛矿相TiO₂。本文中反应介质是酸性的,获得的产品是具有菱形片状结构的锐钛矿相TiO₂,与文献的报道结果一致。

3.3. XPS结果

图3为BTO样品的高分辨XPS谱。图3(a)中的两个峰分别对应于Ti 2p_{3/2}和Ti 2p_{1/2},相应的带能分别为458.8和464.6 eV,这表明TiO₂中Ti的价态为+4价^[33,34]。图3(b)中164.6和159.0 eV处的两个峰分别对应于Bi 4f_{7/2}和Bi 4f_{5/2}的带能,表明在样品中Bi的化学态是+3价^[35]。从图3(c)可以看出,O 1s峰可以分解成带能分别为529.4和530.8 eV的两个峰。前者归属于TiO₂晶格中的Ti–O键;后者的值低于化学吸附水中O–H键的带能(531.5 eV)^[36],我们认为它可能源于Bi–O键^[37]。图3(d)是所有Bi掺杂样品中Cl 2p的XPS谱。可以看出,在198.0和199.6 eV附近有两个峰,分别归属于Cl 2p_{3/2}和Cl 2p_{1/2}^[37,38]。XPS的分析结果,进一步证明了BiOCl相的存在。这与XRD的分析结果是一致的。

3.4. Bi掺杂TiO₂光催化剂的光学吸收

为了阐明Bi掺杂对TiO₂光学性能的影响,我们测试了Bi掺杂TiO₂样品的UV-Vis DRS谱,如图4所示。为了比较,我们也给出了P25的UV-Vis DRS谱。从图4(a)中可

以看出, Bi的掺杂确实影响了TiO₂的光学吸收性能。同P25相比, 130 °C所获得的Bi掺杂TiO₂样品的光吸收一定程度上向可见光区发生了红移。Bi/Ti摩尔比不同, 红移的程度也有所不同。根据上述的XRD和XPS分析结果, Bi离子并没有掺入到TiO₂的晶格中, 而是以BiOCl相的形式存在。因此, 在下面的叙述中, 我们将Bi掺杂TiO₂称为BiOCl复合的TiO₂。然而, 这种新型的BiOCl光催化剂, 带隙为3.2 eV, 只能在紫外区表现出强烈的吸收^[39]。我们课题组以前的研究表明, NTA经水热处理后可以产生大量单电子捕获的氧空位, 这些单电子捕获的氧空位可以在导带下方形成一个子能带, 从而引起可见光的吸收^[40–42]。因此, 我们将BiOCl/TiO₂催化剂对可见光的吸收归因于NTA经水热处理过程中单电子氧空位的形成。图4(b)表明了水热反应温度对BiOCl/TiO₂样品吸收的影响。可以看出, 随着水热反应温度的增加, 这些样品的可见光吸收强度是类似的。这与文献[40]的结果一致。

3.5. 催化剂的光催化活性

BTO催化剂的光催化活性通过甲基橙溶液在可见光下的光降解进行测定。图5为不同催化剂对甲基橙的降解效率。由图5(a)可以看出, 甲基橙在无光照或光催化剂时是很稳定的。还可以看出, P25和纯BiOCl对甲基橙的降解表现出轻微的光催化活性, 这可能是由于少量紫外光残留的原因。当将Bi离子引入TiO₂体系后, 除Bi/Ti摩尔比 = 5%外, 所有复合的样品都对甲基橙的降解表现出较高的光催化活性。同时, BTO样品的光催化活性随着Bi离子量的增加而迅速增加, 当Bi/Ti摩尔比 = 1%时达到最大; 当Bi/Ti摩尔比 = 5%时, 光催化活性反而降低, 并最终降至低于P25的光催化活性。同时, 我们还研究了水热反应温度对光催化性能的影响。从图5(b)可以看出, Bi/Ti摩尔比 = 1%时, 当水热反应温度高于130 °C时, 光催化活性降低。通过以上对比, 我们得知: 最佳Bi/Ti摩尔比为1%, 最佳水热反应温度是130 °C。

图6为甲基橙在不同催化剂上的光降解动力学。可以看出, 在所研究的浓度范围内, 光催化降解遵循准一级动力学反应:

$$\ln(C_0/C_t) = k_{app} \times t$$

式中 k_{app} 是表观一级反应速率常数。对于不同的光催化剂而言, 通常被用作基本的动力学参数, 这是由于根据表观速率常数可以判断光催化活性, 而与甲基橙在暗态的吸附及溶液中残留的甲基橙浓度无关。 $\ln(C_0/C_t)$ 相对于光照时间的变化及相应的表观速率常数 k_{app} 示于图6。可以看出, 可见光照下, BiOCl/TiO₂光催化剂明显增加

了MO光催化降解的表观速率常数。速率常数(或者说光催化活性)遵循下面的顺序: BTO-130-1>BTO-130-0.5>BTO-130-2>BTO-130-0>P25>BTO-130-5。也就是说, BTO的速率常数首先伴随着Bi/Ti摩尔比的增加而增加, 当Bi/Ti摩尔比 = 1%时达到最大。然而伴随着Bi离子量的进一步增加, 速率常数降低, 最终降至和P25类似; 尤其是对于BTO-130-5样品, 甚至比P25还要低。

图5和图6的结果表明, 过量的Bi离子会导致甲基橙光降解效率的降低, 这可能源于过量的BiOCl相的形成。XRD和XPS分析结果表明, Bi离子并没有掺入到TiO₂的晶格中, 而是以BiOCl相的形式存在。而且, 较高的Bi离子量及水热反应温度有助于BiOCl相的产生, 这意味着会有更多的BiOCl相形成。更多的BiOCl相在TiO₂表面上沉积阻止了光生电子和空穴向表面的转移, 并且更多量的BiOCl会形成复合中心, 光诱导的载流子能够被捕获, 从而导致光催化活性降低^[43]。正如图5所示, 未掺杂的TiO₂和纯BiOCl在可见光照下表现出较低的光催化活性。然而, 当Bi/Ti摩尔比从0.5%到1%时, 形成的BTO催化剂却表现出比TiO₂和纯BiOCl高的光催化活性, 这可能同这两种半导体不同的能带位置有关。根据文献[39,44], BiOCl的价带和导带位置都低于TiO₂, 正是由于能带位置的不同加速了光生载流子的转移和分离过程^[45], 从而诱导了更佳的光催化活性。这可能是由于BiOCl的形成给TiO₂引入了晶格缺陷, 产生了更多的光催化活性位。

我们也以钛酸四丁酯为钛源, 采用溶胶-凝胶法将Bi离子引入TiO₂ (所得样品标记为Bi-TiO₂)。其中Bi/Ti摩尔比为1%, 并将其光催化性能同相同摩尔比水热法所制备的BTO催化剂进行比较(图7)。众所周知, 水热法是一种新型的在密封的高温高压环境下制备金属离子掺杂氧化物的技术^[46]。不同于传统的溶胶-凝胶法, 水热法具有很多优点, 比如节约能源, 制备简单, 反应迅速以及较低的操作温度等。如图7所示, 水热法所制备的BTO催化剂的光催化活性高于溶胶-凝胶法制备的Bi-TiO₂催化剂。

同时, 我们又选择了另外一种污染物4-氯苯酚, 考察了BTO-130-1样品的可见光催化性能(图8)。4-氯苯酚的光降解实验在100 mL的光催化反应器中进行, 催化剂的加入量为0.1 g, 4-氯苯酚的初始浓度为12 mg/L。光照前, 光催化剂和4-氯苯酚溶液的混合物首先于暗态维持2 h以达到吸附-脱附平衡。可见光照时间为6 h, 每间隔1 h取样并立即进行离心分离。光催化活性通过监控4-氯苯酚在波长227 nm处吸光度的变化进行评价。可以看

出, 可见光照6 h后, 4-氯苯酚的吸光度明显降低。这表明所获得的BTO光催化剂对有机污染物4-氯苯酚的光降解也表现出较高的光催化活性。

3.6. MO在BTO样品上光催化降解的机理

基于上述分析, BTO催化剂所拥有的高光催化活性归因于NTA水热过程中单电子氧空位在 TiO_2 晶格中的产生以及复合物的形成。形成的单电子氧空位将 TiO_2 的吸收扩展到了可见光区, 而 $\text{BiOCl}/\text{TiO}_2$ 复合物的形成则促进了光生载流子的转移和分离, 二者之间的协同作用促进了光催化活性的提高。据报道, 带隙为3.2 eV的 BiOCl 的价带边和导带边的位置分别为3.44和0.24 eV^[39], 这意味着其价带和导带的能级低于 TiO_2 ^[44]。据此我们提出了甲基橙在复合光催化剂上可能的降解机理。为了阐明光催化降解的机理, 我们首先通过加入不同类型的活性物种捕获剂观察MO的降解效率, 结果如图9所示。当加入甲醇捕获光生空穴或者苯醌捕获超氧自由基负离子($\text{O}_2^{\cdot-}$)以及对苯二甲酸捕获羟基自由基(OH^{\cdot})时, MO的去除率明显降低, 然而当向反应体系中加入硝酸银以捕获光生电子时, MO的降解率急剧增加。这表明, 除了光生电子外, 超氧自由基负离子和羟基自由基以及光生空穴都是甲基橙降解过程中的活性物种。据此, 我们提出了BTO催化剂的催化反应的机理, 如图10所示。在可见光照下, TiO_2 价带的电子首先被激发到由单电子氧空位所形成的子能带上并被单电子氧空位捕获; 随后, 捕获的电子能够被可见光进一步激发到 TiO_2 的导带

上, 并且, 这些电子能够从 TiO_2 的导带转移至 BiOCl 的导带, 相对于单一半导体而言, 这个过程促进了光生电子-空穴对更加有效的分离及较快的表面电荷转移, 而且电子和空穴的复合得到了有效的抑制。在液相介质中, 激发的电子和转移的电子能够被表面吸附的分子氧(O_2)捕获形成超氧自由基负离子, 而价带中的光生空穴能够被吸附在催化剂表面的羟基(OH^{\cdot})或者水分子捕获形成羟基自由基。这两种自由基都是极强的氧化剂足以将有机污染物降解。同时, 具有强氧化能力的光生空穴能够直接氧化MO, 导致随后的降解。因此, BTO光催化剂对MO在可见光下的降解表现出较高的光催化活性。

4. 结论

以NTA为铁源, 采用水热法制备了一系列具有不同 Bi/Ti 摩尔比的Bi掺杂 TiO_2 光催化剂。测试结果表明, Bi离子并没有进入 TiO_2 的晶格, 而是以 BiOCl 相的形式存在于 TiO_2 的表面, 形成 $\text{BiOCl}/\text{TiO}_2$ 复合物。所得样品为拥有菱形片状结构的锐钛矿相。甲基橙的可见光催化降解表明, 这种复合的 TiO_2 样品相对于P25而言有着较高的催化活性。高的光催化活性是由单电子捕获的氧空位和 $\text{BiOCl}/\text{TiO}_2$ 复合物共同引起的。NTA水热处理过程中单电子氧空位的形成促进了可见光的敏化, 而形成的 $\text{BiOCl}/\text{TiO}_2$ 复合物则促进了光生电子和空穴的分离, 阻止了它们的复合。此外, 所制备的复合光催化剂对4-氯苯酚的降解也表现出较高的光催化活性。